Optimal Laser Wavelength for Femtosecond Ionization of Polycyclic Aromatic Hydrocarbons and Their Nitrated Compounds in Mass Spectrometry

Li, Adan
College of Environmental and Chemical Engineering, Yanshan University

Imasaka, Tomoko
Department of Environmental Design, Graduate School of Design, Kyushu University

Imasaka, Totaro
Division of International Strategy, Center of Future Chemistry, Kyushu University

出版情報：Analytical chemistry. 90 (4), pp.2963-2969, 2018-01-29. American Chemical Society
バージョン：
権利関係：

Optimal Laser Wavelength for Femtosecond Ionization of Polycyclic Aromatic Hydrocarbons and their Nitrated Compounds in Mass Spectrometry

Adan Li,[†,‡,*] Tomoko Imasaka,[§] Totaro Imasaka[‡]

[†] College of Environmental and Chemical Engineering, Yanshan University, 438 Hebei Street, Qinhuangdao 066004, China

[‡] Division of International Strategy, Center of Future Chemistry, Kyushu University, 744 Motooka, Nishi-ku, Fukuoka 819-0395, Japan

[§] Department of Environmental Design, Graduate School of Design, Kyushu University, 4-9-1 Shiobaru, Minami-ku, Fukuoka 815-8540, Japan

* To whom correspondence should be addressed. E-mail: arden119@163.com; adan@cstf.kyushu-u.ac.jp

ABSTRACT: The ionization and fragmentation processes were examined for a standard sample mixture containing 16 polycyclic aromatic hydrocarbons (PAHs) and 3 nitro-PAHs (NPAHs) by gas chromatography combined with mass spectrometry (GC/MS) using a femtosecond laser emitting at 400, 800, or 1200 nm as the ionization source. The signal intensities of NPAHs were lower and the fragmentation more extensive compared to those values for PAHs, especially at shorter wavelengths (400 nm). These results can be explained by efficient intersystem crossing to triplet levels and the shorter excited-state lifetimes of neutral NPAHs molecules, compared to the pulse width of the laser. Fragmentation was significantly suppressed by nonresonant multiphoton ionization when a laser emitting at longer wavelengths (1200 nm) was used. This result can be explained by the absorption spectrum of the molecular ion and the excess energy remaining in the ionized state. In fact, there was no absorption band at 1200 nm for the molecular ion and the excess energy would be minimal when a near-infrared laser is used, which suppresses the fragmentation even for NPAHs. A doubly-charged molecular ion was observed for PAHs but not for NPAHs, probably owing to the higher stability of the PAH molecule, the electrons of which are more strongly bound and are more resistive to field ionization. To demonstrate the utility of this technique, the sample extracted from particulate matter 2.5 (PM2.5) emitted from a diesel engine was measured. NPAHs as well as PAHs were clearly determined at 1200 nm, at which the background signal arising from the interference was drastically suppressed.

Epidemiological studies have clearly shown that fine, respirable ambient particular matter (PM) represents a serious health hazard.[1,2] For example, particles with diameters of less than 2.5 μm, referred to as PM2.5, are strongly associated with mortality due to the fact that they contain various aromatic compounds, e.g. polycyclic aromatic hydrocarbons (PAHs) and nitrated polycyclic aromatic hydrocarbons (NPAHs), which are suspected to be mutagenic and carcinogenic. The concentrations of NPAHs that are adsorbed on PM2.5 in ambient air are 10 to 100 times lower than those of PAHs.[3] The mutagenicity and carcinogenicity of NPAHs are, however, 10-10000 times higher than those of the corresponding PAHs.[4] Since PM2.5 also contains high levels of numerous interfering organic compounds, a sensitive and selective analytical method is desirable for the determination of PAHs and NPAHs.

Analytical techniques such as gas chromatography/mass spectrometry (GC/MS),[5,6] comprehensive two-dimensional gas chromatography/mass spectrometry (GC×GC/MS),[7] and liquid chromatography/mass spectrometry (LC/MS)[8,9] have been applied to unravel the constituents of the complex organic compounds in ambient aerosol particles as well as particulate matter collected from various emission sources such as industrial combustion facilities. However, these methods suffer from limited selectivity in MS based on electron ionization, and tedious and time-consuming sample pretreatment processes are required. A photoionization (PI) technique is recently developed that improves the selectivity of this method, in which there are two major approaches: (i) single photon ionization (SPI) using a vacuum-ultraviolet (VUV) light source for the detection of aromatic and aliphatic compounds,[10-12] (ii) multiphoton ionization (MPI) using intense ultraviolet (UV), visible (VIS), and even near-infrared (NIR) lasers for the detection of various compounds, including PAHs and NPAH. [13-19]

In SPI, the molecule can be ionized only when it absorbs a photon whose energy exceeds the ionization energy. Then, this technique can be used to detect specific aromatic and aliphatic compounds. The energy of photons that are typically used in the experiment (10.5 eV, 118 nm) is

larger than the ionization threshold for most organic compounds, thus making it soft ionization that produces little or no fragments in MS. In MPI, at least two photons are required for ionization. When a molecule is ionized via an intermediate state, referred to as resonance-enhanced MPI (REMPI), sensitivity and selectivity can be improved significantly by using a laser with the optimal wavelength for ionization. An advantage of this technique is that aromatic compounds in a complex matrix obtained from an environmental sample can be detected. For this reason, a UV laser has been successfully used for the sensitive as well as selective ionization of PAHs, NPAHs, dioxins, and pesticides.[13,14] However, the excess energy associated with ionization cannot be minimized, due to a mismatch between the photon energy, i.e., the wavelength of the laser, and the 0-0 (singlet-singlet) transition energy from the electronically ground state to the lowest singlet excited state of the neutral molecule (*EX*) that depends on the molecule to be measured. Thus, the excess energy remaining in the molecular ion cannot be decreased for all the analyte molecules. This unfavorable effect can be minimal by using nonresonant MPI (NRMPI), the resonance effect of which is insignificant at short pulse width (< ca. 70 fs).[21] In order to optimize sensitivity and selectivity in MPI,[13-17,19] femtosecond lasers emitting in the far- (200 nm), deep- (267 nm), and near-UV (345 nm) regions are employed for the detection of PAHs and amino- and nitro-derivatives thereof.[13] Ionization efficiency in two-photon REMPI can be significantly improved by using a far-UV laser, thus making it useful for the more sensitive detection of standard molecules. However, the use of a near-UV laser (345 nm) for the trace analysis of a real sample, which was based on one-photon excitation followed by two-photon ionization (1 + 2 REMPI), would be useful for suppressing background signals arising from interfering substances that are present in PM2.5. In our previous study, we compared UV and NIR lasers for use in efficient ionization and for observing a molecular ion of pentachlorobenzene.[22] To our knowledge, no systematic studies have been reported to date regarding finding an optimal laser wavelength for the femtosecond ionization of PAHs and their corresponding NPAHs in MS except the studies for several single-ring aromatic molecules.[23,24]

In this study, we report on an examination of the ionization and fragmentation processes using a standard sample mixture containing 16 PAHs specified by the United States Environmental Protection Agency (US EPA) and 3 NPAHs. We employed femtosecond lasers emitting at 400, 800, and 1200 nm with laser intensity of 1.2×10^{14}, 6.0×10^{13}, and 2.8×10^{13} W/cm^2, respectively, to determine the optimal wavelength needed for efficient ionization and for observing a molecular ion. The obtained results were correlated with spectral data for the molecular ion derived by quantum chemical calculations. The present analytical instrument was applied to the analysis of a sample (SRM 1975) extracted from the particulate matter emitted from a diesel engine.

EXPERIMENTAL SECTION

Reagents and chemicals. A standard sample mixture of PAHs listed in the priority table of the US EPA, i.e., acenaphthene (ACE), acenaphthylene (ACY), anthracene (ANT), benzo(a)anthracene (BaA), benzo(b)fluoranthene (BbF), benzo(k)fluoranthene (BkF), benzo(ghi)perylene (BPY), benzo(a)pyrene (BaP), chrysene (CHR), dibenzo(a,h)anthracene (DBA), fluoranthene (FLT), fluorene (FLU), indeno(1,2,3-cd)pyrene (IND), naphthalene (NAP), phenanthrene (PHE), and pyrene (PYR), was prepared at a concentration of 500 pg/μL for each compound using a (1:1 v/v) solvent mixture of methylene chloride and benzene (Supelco, Bellefonte, PA, USA). A standard sample mixture of 9-nitro-anthracene (9-NANT), 3-nitro-fluoranthene (3-NFLT), and 1-nitro-pyrene (1-NPYR) dissolved in toluene (500 pg/μL for each compound) was purchased from AccStandard Inc. New Haven, CT, USA. The standard sample mixture used in this study was prepared by mixing the above two standard samples at a volume ratio of 1:1 (i.e. 250 pg/μL for each compound).

Standard Reference Material 1975 (SRM 1975) is intended for use in evaluating an analytical method used for the determination of PAHs and NPAHs in diesel particulate matter. All of the sample solutions measured in this study were stored in an amber-colored glass container at 4 °C.

Analytical grade toluene and methanol were purchased from the Kanto Chemical Co., INC. Tokyo, Japan.

Apparatus. A schematic diagram of the experimental apparatus is shown in Figure 1. The fundamental beam of a Ti:sapphire laser (800 nm, 35 fs, 1 kHz, 4 mJ, Elite, Coherent Co., Santa Clara, CA, USA) was used as a pump source for an optical parametric amplifier (OPA, 35 fs, 1 kHz, OPerA-Solo, Coherent Co.). The fundamental (800 nm) or second harmonic (400 nm, 37 fs) beam of the Ti:sapphire laser, or the signal beam of the OPA (1200 nm, 35 fs) was focused by a concave mirror with a focal length of 50 cm onto a molecular beam in a linear-type time-of-flight mass spectrometer (TOF-MS) (HGK-1, Hikari-GK, Fukuoka, Japan). The polarization of the laser beams emitting at 400 and 1200 nm was rotated by 90 degrees using a half-wave plate to adjust the direction of polarization so as to make it the same as to that of the beam emitting at 800 nm (*p*-polarization), which was in parallel to the direction of the flight tube. The pulse energy of the laser beam emitting at 400, 800, and 1200 nm was measured in front of the input window of the MS using a power meter commercially available (FieldMate, Coherent Inc.). The ions induced by MPI were measured by an assembly of microchannel plates (MCP, F4655-11, Hamamatsu Photonics, Shizuoka, Japan), the voltages applied to the input and output electrodes of the MCP being 2000 and 334 V, respectively. In this study, the absolute value of the signal intensity was expressed in a unit of mV, since it is useful to compare the signal intensities and also to check the signal saturation of the MCP detector. The mass spectrum was recorded using a digitizer (AP240, 1 GHz, 1 GS/s, Acqiris, Agilent Technologies, Santa Clara, CA, USA).

A 1-μL aliquot of sample solution was injected into a GC system (6890N, Agilent Technologies, Santa Clara, CA, USA) using an auto sampler (7683B, Agilent Technologies) to separate the compounds on a capillary column (DB-5ms, 30 m, 0.25 mm id., 0.25 μm film thickness, Agilent Technologies). The temperature program of the GC oven was set to increase from 60 °C (1 min

hold) to 120 °C (1 min hold) at a rate of 20 °C/min and then to 280 °C (10 min hold) at 5 °C/min. The data were analyzed using the LabVIEW software. The temperature of the transfer line was maintained at 300 °C. The signal intensity was calculated from the mass spectral data using software programmed by LabVIEW.

Quantum calculations. Quantum chemical calculations were performed to gain insights into the ionization mechanism of cationic species produced from PYR and 1-NPYR using a Gaussian 09 program series package. Minimum geometries were obtained using the B3LYP method based on density functional theory (DFT) with a cc-pVDZ basis set.[25] The harmonic frequencies were calculated so as to ensure an optimum geometry for providing a global energy minimum. A vertical ionization energy (*IE*) was evaluated from the difference between the energies of the ground and ionic states. The lowest 40 singlet transition energies and the oscillator strengths were calculated using time-dependent DFT (TD-DFT),[26] and the predicted absorption spectra were generated using the GaussView 5 software program by assuming a spectral line having a Gaussian profile with a full width at half maximum of 0.333 eV for each transition.

RESULTS AND DISCUSSION

Ionization Mechanism. Figure 2 shows two-dimensional displays against the retention time and the *m/z* values for the standard sample mixture containing 16 PAHs and 3 NPAHs measured using lasers emitting at 400, 800, and 1200 nm, the pulse energies of which were 80, 180, and 180 μJ, respectively. The laser intensity at the focal point was then calculated to be 1.2×10^{14}, 6.0×10^{13} and 2.8×10^{13} W/cm^2: the position of the concave mirror for focusing the beam onto the molecular beam was translated by *ca.* 3 mm to obtain the maximum signal intensity for the molecular ion by introducing pentachlorobenzene as a sample. Then, the actual laser intensity would be slightly lower than these values (*e.g.* $2.80\rightarrow2.76\times10^{13}$ W/cm^2 at 1200 nm). Two ionization schemes are possible,

i.e., MPI and field ionization (FI). The parameter of $\gamma = (E_i / 1.87\times10^{-13} I\lambda^2)^{1/2}$, defined by Keldysh, can be used to separate these regimes, where E_i is the zero-field ionization potential expressed in eV, I is the laser intensity in W/cm^2, and λ is the laser wavelength in a unit of μm.[27] When $\gamma \ll 1$, FI prevails. On the other hand, MPI is dominant at $\gamma \gg 1$. The effect of FI appears to be significant when a higher-intensity laser emitting at a longer wavelength was tightly focused on the sample. The γ value calculated from the laser intensity and the *IE* values for all of the compounds examined in this study (see Table 1) was 1.4-1.5 at 400 nm, 1.0-1.1 at 800 nm, and 0.97-1.0 at 1200 nm. The values are equal to or slightly larger than 1, suggesting that PAHs and NPAHs are ionized in the boundary region of MPI and FI (or slightly shifted to MPI). The expanded views of the parts where FLT and PYR (*m/z* = 202), and NFLT and NPYR (*m/z* = 202) appear are shown in Figure 3. The compounds investigated here were well resolved by GC and identified by MS, and the molecular ions were clearly observed as the major ions.

The spectral properties, possible ionization schemes, and the signal intensities observed for ANT, FLT, and PYR, and their corresponding NPAHs are summarized in Table 1. The *IE* values were in the range of 7.43-8.06 eV, with *EX* values in the range of 2.76-3.34 eV. The energy of one photon (3.10 eV) at 400 nm would be sufficient for 1+2 MPI except for ANT and PYR (2+1 MPI). On the other hand, more than 5 photons are required for ionization at 800 nm and more than 7 photons at 1200 nm.

Ionization Efficiency. In general, the ionization efficiency decreases with increasing numbers of photons required for MPI. The ionization efficiency obtained at 1200 nm, which requires 7-8 photons, should therefore be lower than those obtained at 400 and 800 nm, for which 3-5 photons are required. However, due to the high laser intensity of the laser used in this study (6.0×10^{13}, 2.8×10^{13} W/cm^2), no significant difference was observed for the signal intensities of the molecular ion (M^+) measured at the different wavelengths. In fact, the intensities of M^+ measured at 400 nm were lower

than those measured at 800 and 1200 nm in most cases (see Table 1), suggesting that the molecules are ionized in the nonlinear (saturated) region against the laser intensity. The observed values of M^+/F^+ (ratio of the signal intensities for the molecular ion and the largest fragment ion observed in the mass spectrum) suggest that fragmentation appears to be efficient when a laser emitting at shorter wavelengths (e.g., 400 nm) is used.

The ionization efficiency for NPAHs was generally poorer than that for PAHs, as shown in Table 1. The lower values of M^+/F^+ of NPAHs comparing with PAHs suggest that NPAHs had undergone efficient fragmentation, resulting in the decreasing of the intensities for molecular ions. An NO_2 group attached to PAH can be easily dissociated to generate fragment ions, as reported in mass spectra compiled in the NIST Standard Reference Database for PAHs and their corresponding NPAHs.[30] Nanosecond and femtosecond lasers have been utilized for ionization in the MS of NPAHs to explore the photo-dynamics associated with the loss of NO_2 and the formation of NO^+ from the molecular ion.[31-33] In these studies, the efficient photo-dissociation of NPAHs and the advantage of using a femtosecond laser in the ionization have been reported. It should be noted that the presence of an NO_2 group significantly decreases the exited-state lifetimes of such neutral NPAHs molecules (ca. 10^5 - 10^6 fold shorter than those of PAHs). As a result, the lifetimes decrease to 50-540 fs (see Table 1); the lifetimes of 9-NANT and 3-NFLT are nearly identical to the pulse width of the laser (ca. 35 fs) used in this study, resulting in efficient intersystem crossing to triplet levels of the neutral molecules. These lifetime values of NPAHs would decrease the efficiency of ionization. In fact, the intensities of the M^+ ion for ANT, FLT, and PYR were 68, 228 and 295 mV while the values for their corresponding NPAHs were 17, 14 and 19 mV at 400 nm. The trend of decreasing of the signal intensity for the M^+ of NPAH compared to corresponding PAHs remained unchanged even when a laser emitting at 800 and 1200 nm was used.

Fragmentation. Figure 4 shows mass spectra for PYR and 1-NPYR measured at 400, 800, and 1200 nm. From the mass/charge ratio, *m/z*, some of the signal peaks measured for 1-NPYR can be assigned to fragment ions of $[M\text{-}NO\text{-}CO]^+$ (m/z = 189), $[M\text{-}NO_2]^+$ (201), and $[M\text{-}NO]^+$ (217), these assignments of which were confirmed by using a previously reported database.[34-36] Fragmentation of PYR was more extensive at 400 nm than at 800 and 1200 nm. These findings can be explained by two factors. One would be the larger excess energy (3.10 eV×3 - 7.43 eV= 1.87 eV) at 400 nm than the value (0.32 eV) at 800 nm and the value (0.71 eV) at 1200 nm. Another would be the dissociation of the molecular ion by absorbing additional photons. In fact, a molecular ion can be efficiently dissociated when it has an absorption band at the wavelength of the laser being used.[22,37-39] The absorption spectrum was then calculated for the ionic state of PYR and 1-NPYR based on TD-DFT calculations. The results are shown in Figure 5. In the first step, the neutral molecule is ionized by absorbing several photons to produce a singly-charged M^+ ion. This process would be more efficient at 400 nm through the process of 1 + 2 REMPI, since NRMPI is required for ionizations at 800 and 1200 nm. The calculated absorption spectra suggest that the molecular ion efficiently absorbs subsequent photons at 400 nm (molar absorptivity; 0.80×10^4 $M^{-1}cm^{-1}$ for PYR and $1.2\times10^4$for 1-NPYR) but the process is inefficient at 800 nm (molar absorptivity; 0.02×10^4 $M^{-1}cm^{-1}$ for PYR and 0.23×10^4 $M^{-1}cm^{-1}$ for 1-NPYR). This trend was nearly identical to that for the other PAHs and NPAHs. Since there is no absorption band at above 1000 nm, the molecular ion is difficult to dissociate by absorbing another photon at 1200 nm. Thus, fragmentation would be strongly affected by the absorption characteristics of the molecular ion at the laser wavelength being used.[40-43] This consideration is very different from the ionization that occurs in the UV region, where the signal increase by REMPI and the use of more moderate conditions (e.g., low pulse energy) are key issues in enhancing the molecular ion.[13,28]

As recognized from Table 1, the M^+/F^+ value depends on the laser wavelength. For example, the ratio increases 15, 24, and 209 fold when the wavelength changes from 400 to 1200 nm. A similar

trend was observed for the other NPAHs, e.g., the values were 0.68, 0.80, and 8.9 for 9-NANT at 400, 800, and 1200 nm, respectively. As demonstrated herein, fragmentation was substantially suppressed when an NIR laser (1200 nm) was used as the ionization source.

In addition to a singly-charged molecular ion and fragment ions, a doubly-charged ion was observed for PAHs such as BaA, CHR, BbF, BkF, BaP, IND, DBA, and BPY, due to the high laser intensity employed in this study. Mass spectra showing the doubly-charged ion of BPY measured at 400, 800, and 1200 nm are shown in Figure 6. The assignment of the doubly-charged ion was confirmed from the pattern of the isotope peaks (e.g., m/z = 138.5) arising from ^{13}C-BPY (see the expanded view shown as an insert in Figure 6). Moreover, the peak width of the doubly-charged ion was much narrower than those of the other fragment ions due to a narrower distribution of the kinetic energy of the molecular ion than those of the fragments formed by dissociation of the neutral/ionic species. Note that such the doubly-charged ion has been observed for several PAHs, e.g., naphthalene, triphenylene, and coronene, under strong radiation field.[44,45] Multiply-charged ions would appear by FI; for example, Xe^{2+} was firstly observed in 1983 and was followed by the observation of Xe^{26+} in 2003 at 10^{19} W/cm^2.[46,47]

Actual sample. A sample of SRM 1975 that was intended for use in evaluating the optimal laser wavelength for the determination of PAHs and NPAHs in diesel particulate matter was used as an actual sample. Two-dimensional displays observed at 400, 800, and 1200 nm are shown in Figure 7. Numerous signal peaks were observed at 400 nm, in contrast to the data observed at 1200 nm. Most of these signals can be attributed to interfering substances contained in the matrix of the real sample (cf. Figure 2). These data indicate that the NIR laser is useful for suppressing the intensity of undesirable signals in the two-dimensional display. As mentioned, trace analysis of PAHs and NPAHs has been examined in the previous studies using the laser emitting in the UV region (200-405 nm).[13,28] The background signal was lower at longer wavelengths, which was preferential for the

measurement of the actual sample, suggesting optimal ionization at 1200 nm. The signal intensities of the molecular ions for PAHs and NPAHs are summarized in Table 2: the signal peaks were assigned from the retention times and the *m/z* values obtained using the standard sample and are marked in Fig. 7 (C). As shown in Table 2, no significant differences were found among the data measured at 400, 800 and 1200 nm, although the relative sensitivity (selectivity) is strongly dependent on the molecule being measured. The reasonable signal intensities for the molecular ions and efficient background suppression suggest that the use of an NIR laser (1200 nm), especially for a real sample containing a variety of interference species, represents an ideal set up for measuring such substances.

CONCLUSIONS

In this study, 16 PAHs and 3 NPAHs were measured by TOF-MS using a femtosecond laser as the ionization source at 400, 800, and 1200 nm. A molecular ion was measured as the major ion for PAHs, while a series of fragment ions were observed more dominantly at 400 nm for NPAH, which contain a dissociable NO_2 group. However, fragmentation was significantly suppressed and a molecular ion was clearly observed as a major ion at 1200 nm. This desirable result can be attributed to the small excess energy (0.71 eV) remaining in the molecular ion and the absence of an absorption band at the laser wavelength. This finding suggests that a femtosecond laser emitting in the NIR region (1200 nm) can be successfully used for the analysis of trace amounts of PAHs and NPAHs. We conclude that similar results would likely be obtained for the other PAHs with different substituent groups, e.g., -NO, -OH, $-C_nH_{2n+1}$, which are also suspected to be strongly carcinogenic and mutagenic and present in the environment, although further studies based on quantum chemical calculations would be necessary to verify this. It should be noted that a high-power, low-cost, compact, robust, easy-to-use, femtosecond NIR laser based on optical fiber technology is commercially available and can be directly used without any harmonic generation system. Thus, this

technique has the potential for use in the practical trace analysis of PAHs and analogs thereof in the environment where numerous interfering species are present at high concentrations.

AUTHOR INFORMATION

Corresponding Author

* E-mail: arden119@163.com

ORCID

Adan Li: 0000-0002-5803-2457

Totaro Imasaka: 0000-0003-4152-3257

Notes:

The authors declare no competing financial interest.

ACKNOWLEDGMENTS

This research was supported by a grant from the National Natural Science Foundation of China (No. 21407126) and by a Grant-in-Aid for Scientific Research from the Japan Society for the Promotion of Science (JSPS KAKENHI Grant Numbers JP26220806 and JP15K01227). The computations were mainly carried out using the computer facilities at the Research Institute for Information Technology, Kyushu University.

REFERENCES

(1) Pope, C. A.; Burnett, R. T.; Thun, M. J.; Calle, E. E.; Krewski, D.; Ito, K.; Thurston, G. D., *J. Am. Med. Assoc.* **2002**, *287*, 1132–1141.

(2) Brook, R. D.; Brook, J. R.; Urch, B.; Vincent, R.; Rajagopalan, S.; Silverman, F. *Circulation* **2002**, *105*, 1534–1536.

(3) Hayakawa, K.; Murahashi, T.; Butoh, M.; Miyazaki, M. *Environ. Sci. Technol.* **1995**, *29*, 928–932.

(4) Durant, J. L.; Busby, W. F.; Lafleur, A. L.; Penman, B. W.; Crespi, C. L. *Mutat. Res. Genet. Toxicol.* **1996**, *371*, 123–157.

(5) Zheng, M.; Salmon, L. G.; Schauer, J. J.; Zeng, L.; Kiang, C. S.; Zhang, Y.; Cass, G. R. *Atmos. Environ.* **2005**, *39*, 3967–3976.

(6) Rogge, W. F.; Hildemann, L. M.; Mazurek, M. A.; Cass, G. R. *Environ. Sci. Technol.* **1993**, *27*, 636–651.

(7) Fushimi, A.; Hashimoto, S.; Ieda, T.; Ochiai, N.; Takazawa, Y.; Fujitani, Y.; Tanabe, K. *J. Chromatogr. A* **2012**, *1252*, 164–170.

(8) Colombini, M. P.; Fuoco, R.; Giannarelli, S.; Termine, M.; Abete, C.; Vincentini, M.; Berti, S. *Microchem. J.* **1998**, *59*, 228–238.

(9) Schauer, C.; Niessner, R.; Pöschl, U. *Anal. Bioanal. Chem.* **2004**, *378*, 725–736.

(10) Ferge, T.; Mu1hlberger, F.; Zimmermann, R. *Anal. Chem.* **2005**, *77*, 4528–4538.

(11) Woods, E.; Smith, G. D.; Dessiaterik, Y.; Baer, T.; Miller, R. E. *Anal. Chem.* **2001**, *73*, 2317–2322.

(12) Öktem, B.; Tolocka, M. P.; Johnsten, M. V. *Anal. Chem*. **2004**, *76*, 253–261.

(13) Tang, Y. Y.; Imasaka, T.; Yamamoto, S.; Imasaka, T. *Talanta* **2015**, *140*, 109–114.

(14) Li, A.; Uchimura, T.; Tsukatani, H.; Imasaka, T. *Anal. Sci.* **2010**, *26*, 841–846.

(15) Bente, M.; Adam, T.; Ferge, T.; Gallarvardin, S.; Sklorz, M.; Zimmermann, R. *Int. J. Mass Spectrom.* **2006**, *258*, 86–94.

(16) Gittins, C. M.; Castaldi, M. J.; Senkan, S. M.; Rohlfing, E. A. *Anal. Chem.* **1997**, *69*, 286–293.

(17) Boesl, U. J. *Mass Spectrom.* **2000**, *35*, 289–304.

(18) Levis, R. J.; DeWitt, M. J. *J. Phys. Chem. A* **1999**, *103*, 6493–6507.

(19) Ledingham, K. W. D.; Singhal, R. P. *Inter. J. Mass Spectrom. Ion Process.* **1997**, *163*, 149–168.

(20) Haefliger, O. P.; Zenobi, R. *Anal. Chem*. **1998**, *70*, 2660–2665.

(21) Kouno, H; Imasaka, T. *Analyst* **2016**, *141*, 5274–5280.

(22) Li, A.; Phan, D. T.; Imasaka, T.; Imasaka, T. *Analyst* **2017**, *142*, 3942-3947.

(23) Bohinski, T.; Tibbetts, K. M.; Munkerup, K.; Tarazkar, M.; Romanov, D. A. *Chem. Phys.* **2014**, *442*, 81–85.

(24) Tanaka, M.; Kawaji, M.; Yatsuhashi, T., Nakashima, N. *J. Phys. Chem. A* **2009,** *113*, 12056–12062.

(25) Dunning, T. H. J. *Chem. Phys. Lett.* **1989**, *90*, 1007–1023.

(26) Bauernschmitt, R.; Ahlrichs, R. *Chem. Phys. Lett.* **1996**, *256*, 454–464.

(27) Keldysh, L. V. *Sov. Phys. JETP* **1965**, *20*, 1307–1314.

(28) Tang, Y. Y.; Imasaka, T.; Yamamoto, S.; Imasaka, T. *Chemosphere* **2016**, *152*, 252–258.

(29) Morales-Cueto, R.; Esquivelzeta-Rabell, M.; Saucedo-Zugazagoitia, J.; Peon, J. *J. Phys. Chem. A* **2007**, *111*, 552–557.

(30) Data compiled from NIST Standard Reference Database, http://webbook.nist.gov/chemistry/form-ser.html.

(31) Dotter, R. N.; Smith, C. H.; Young, M. K.; Kelly, P. B.; Jones, A. D.; McCauley, E. M.; Chang, E. M.; Chang, D. P. Y. *Anal. Chem.* **1996**, *68*, 2319-2324.

(32) Ledingham, K. W. D.; Kilic, H. S.; Kosmidis, C.; Deas, R. M.; Marshall, A.; McCanny, T.; Singhal, R. P.; Langley, A. J.; Shaikh, W. *Rapid Commun. Mass Spectrom.* **1995**, *9*, 1522-1527.

(33) Marshall, A.; Clark, A.; Jennings, R.; Ledingham, K. W. D.; Sander, J.; Singhal, R. P. *Int. J. Mass Spectrom. Ion Process* **1992**, *116*, 143-156.

(34) Bezabeh, D. Z.; Allen, T. M.; McCauley, E. M.; Kelly, P. B. *J. Am. Soc. Mass Spectrom.* **1997**, *8*, 630–636.

(35) Tasker, A. D.; Robson, L.; Ledingham, K. W. D.; McCanny, T.; McKenna, P.; Kosmidis, C.; Jaroszynski, D. A. *Int. J. Mass Spectrom.* **2003**, *225*, 53–70.

(36) Arce, R.; Pino, E.; Valle, C.; Ágreda, J. *J. Phys. Chem. A* **2008**, *112*, 10294–10304.

(37) Konar, A.; Shu, Y.; Lozovoy, V. V.; Jackson, J. E.; Levine, B. G.; Dantus, M. *J. Phys. Chem. A* **2014**, *118*, 11433–11450.

(38) Yatsuhashi, T.; Nakashima, N. *J. Photochem. Photobiol. C: Photochem. Rev.* **2017**, https://doi.org/10.1016/j.jphotochemrev.2017.12.001.

(39) Harada, H.; Shimizu, S.; Yatsuhashi, T.; Sakabe, S.; Izawa, Y.; Nakashima, N. *Chem. Phys. Lett*. **2001**, *342*, 563–570.

(40) Lezius, M.; Blanchet, V.; Ivanov, Y. M.; Stolow, A. *J. Chem. Phys.* **2002**, *117*, 1575–1588.

(41) Tanaka, M.; Panja, S.; Murakami, M.; Yatsuhashi, T.; Nakashima, N. *Chem. Phys. Lett*. **2006**, *427*, 255–258;

(42) Murakami, M.; Tanaka, M.; Yatsuhashi, T.; Nakashima, N. *J. Chem. Phys*., **2007,** *126*, 104304.

(43) Markevitch, A. N.; Smith, S. M.; Romanov, D. A.; Schlegel, H. B.; Ivanov, M. Y.; Levis, R. J. *Phys Rev A* **2003,** *68*, 011402.

(44) Ławicki, A.; Holm, A. I. S.; Rousseau, P.; Capron, M.; Maisonny, R.; Maclot, S.; Seitz, F.; Johansson, H. A. B.; Rosén, S.; Schmidt, H. T.; Zettergren, H.; Manil, B.; Adoui, L.; Cederquist, H.; Huber, B. A. *Phys. Rev. A* **2011**, *83*, 022704.

(45) Yatsuhashi, T.; Nakashima, N. *J. Phys. Chem. A* **2010**, *114*, 7445–7452.

(46) L'Huillier, A.; Lompré, L. A.; Mainfray, G.; Manus, C. *Phys. Rev. A* **1983**, *27*, 2503–2512.

(47) Yamakawa, K.; Akahane, Y.; Fukuda, Y.; Aoyama, M.; Inoue, N.; Ueda, H. *Phys. Rev. A* **2003**, *68*, 065403.

(48) Majcherczyk, A.; Johannes, C.; Hüttermann, A. *Enzyme and Microb. Tech.* **1998**, *22*, 335–341.

Table 1. Spectral properties and observed data for 3 PAHs and their nitro-compounds

Compounds (M.W.)	*IE* (eV)	*EX* (eV)	Ionization Mechanism			τ (fs)	Intensity of M^+ (mV)			M^+/F^+		
			400 nm (3.10 eV)	800 nm (1.55 eV)	1200 nm (1.03 eV)		400 nm	800 nm	1200 nm	400 nm	800 nm	1200 nm
ANT (178)	7.44[a]	3.31[c]	2+1MPI	3+2MPI	4+3MPI	8.0×10^{6} [c]	68	187	167	15	24	209
FLT (202)	7.90[a]	3.06[c]	1+2MPI	2+3MPI	3+5MPI	3.8×10^{7} [c]	228	300	240	24	70	224
PYR (202)	7.43[a]	3.34[c]	2+1MPI	3+2MPI	4+4MPI	1.4×10^{9} [c]	295	355	260	27	93	520
9-NANT (223)	7.86[a]	2.84[b]	1+2MPI	2+3MPI	3+5MPI	60[d]	17	8	34	0.68	0.80	8.9
3-NFLT (247)	8.06[b]	2.76[b]	1+2MPI	2+3MPI	3+5MPI	50[d]	14	12	30	0.56	1.2	2.5
1-NPYR (247)	7.67[b]	3.07[b]	1+2MPI	2+3MPI	3+5MPI	540[d]	19	17	70	0.56	1.2	5.0

[a] Data reported in the NIST Standard Reference Database, March 1998 Release: NIST Chemistry Web Book. [b] ref. 28. [c] ref. 20. [d] ref. 29. The sample was prepared at a concentration of 250 pg/μL. M.W., molecular weight. τ, the lifetime of the electronic excited singlet state of neutral molecule.

Table 2. Assignments of PAHs and NPAHs present in a sample extracted from the diesel particulate matter (SRM 1975)

Elution Order	Compounds (M.W.)	*IE* (eV)	Signal Intensity of M^+ (mV)		
			400 nm	800 nm	1200 nm
1	NAP (128)	8.12[a]	1476	1706	1262
2	ACY (152)	8.22[a]	920	674	219
3	ACE (154)	7.68[a]	nf	nf	nf
4	FLU (166)	7.88[a]	187	173	138
5	PHE (178)	7.90[a]	1462	1442	1435
6	ANT (178)	7.44[a]	312	189	159
7	FLT (202)	7.9[a]	1434	1984	2376
8	PYR (202)	7.43[a]	811	92	62
9	9-NANT (223)	7.59[b]	145	26	387
10	BaA (228)	7.53[a]	101	25	36
11	CHR (228)	7.60[a]	289	94	204
12	3-NFLT (247)	8.06[b]	15	5	26
13	1-NPYR (247)	7.67[b]	156	40	247
14	BbF (252)	7.70[c]	432	501	426
15	BkF (252)	7.48[c]	132	77	78
16	BaP (252)	7.10[a]	43	93	155
17	IND (276)	nf	160	107	139
18	DBA (278)	7.38[a]	14	8	13
19	BPY (276)	7.16[a]	5	6	9

[a] Data reported in the NIST Standard Reference Database. March 1998 Release: NIST Chemistry Web Book. nf: not found. [b] ref. 26. [c] ref. 48. M.W., molecular weight.

Figure captions

Figure 1. Schematic diagram of the experimental apparatus used in this study. OPA: optical parametric amplifier, M: mirror, CM: concave mirror, DM: dichroic mirror, BBO: β-barium borate crystal for second harmonic generation, $\lambda/2$: half-wave plate, BS: beam splitter.

Figure 2. Two-dimension display measured for a standard sample mixture containing 16 PAHs and 3 NPAHs and the total ion chromatogram (TIC) obtained at 1200 nm. Concentration, 250 pg/μL; Pulse energy, 180 μJ. RT, retention time.

Figure 3. Expanded views of the two-dimension display measured for a standard sample mixture containing 16 PAHs and NPAHs in the regions where (A) FLT and PYR (B) 3-NFLT and 1-NPYR appear.

Figure 4. Mass spectra of (A) PYR and (B) 1-NPYR measured at 400, 800, and 1200 nm.

Figure 5. Calculated absorption spectra for a singly-charged ion of (A) PYR (B) 1-NPYR.

Figure 6. Mass spectra of BPY measured at 400, 800, and 1200 nm. Expanded views of the region, where the molecule ion (M^+) and the doubly-charged molecular ion (M^{2+}) appear, are shown as inserts in the mass spectrum measured at 800 nm.

Figure 7. Two-dimension displays measured for SRM 1975 at (A) 400 nm (B) 800 am (C) 1200 nm, and TIC obtained at 1200 nm.

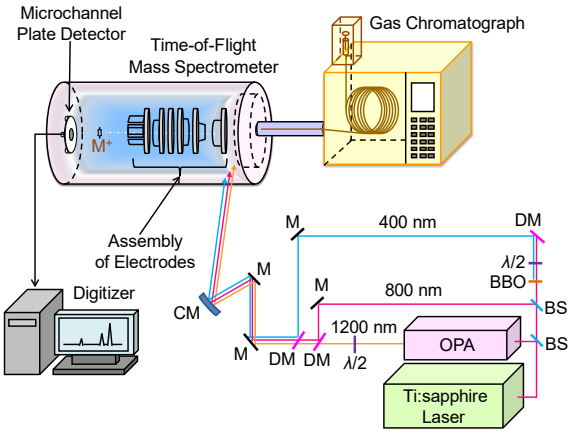

Fig. 1 A. Li et al.

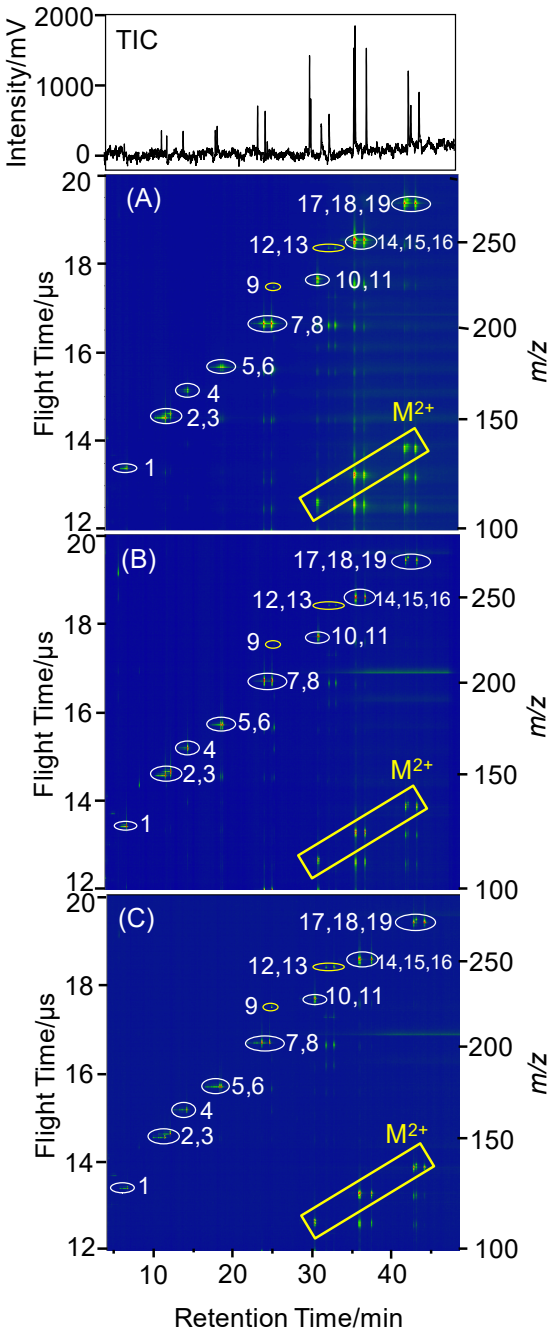

Fig. 2 A. Li et al.

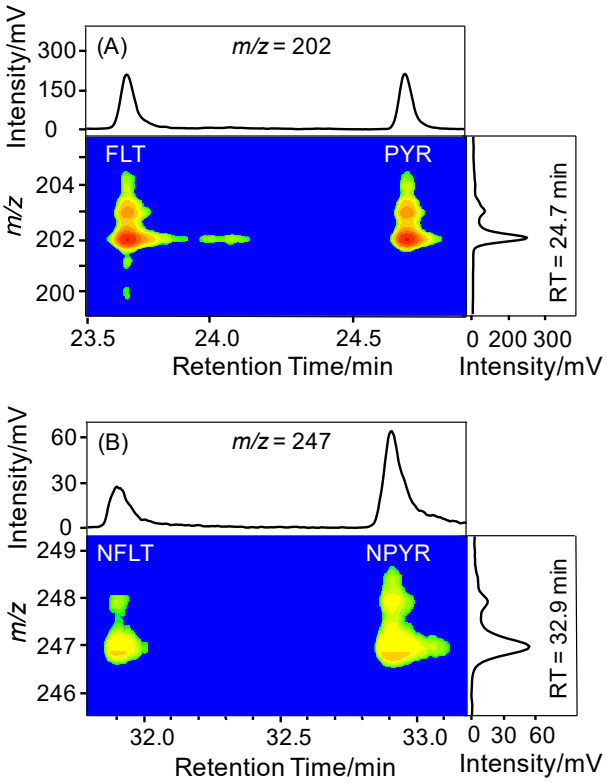

Fig. 3 A. Li et al.

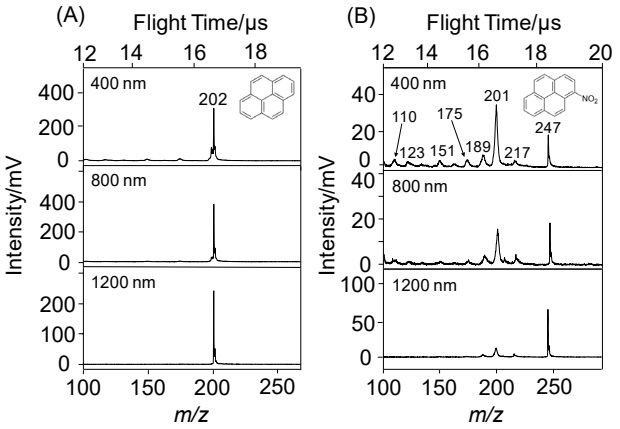

Fig. 4 A. Li et al.

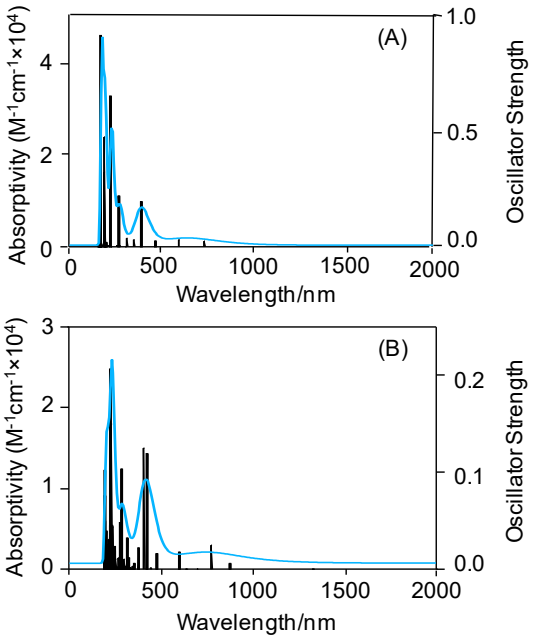

Fig. 5 A. Li et al.

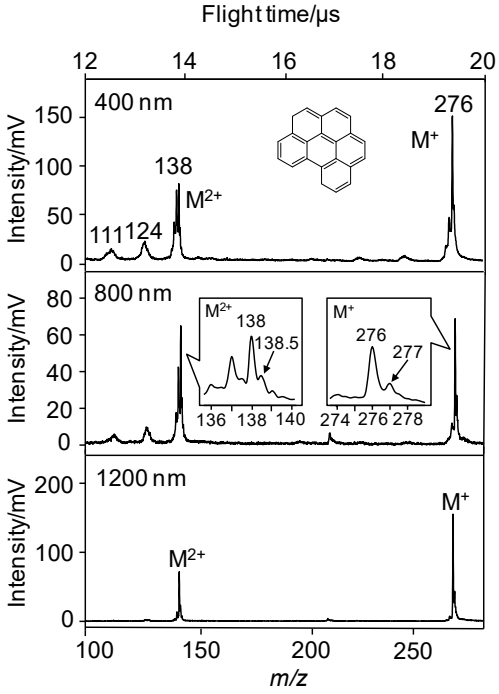

Fig. 6 A. Li et al.

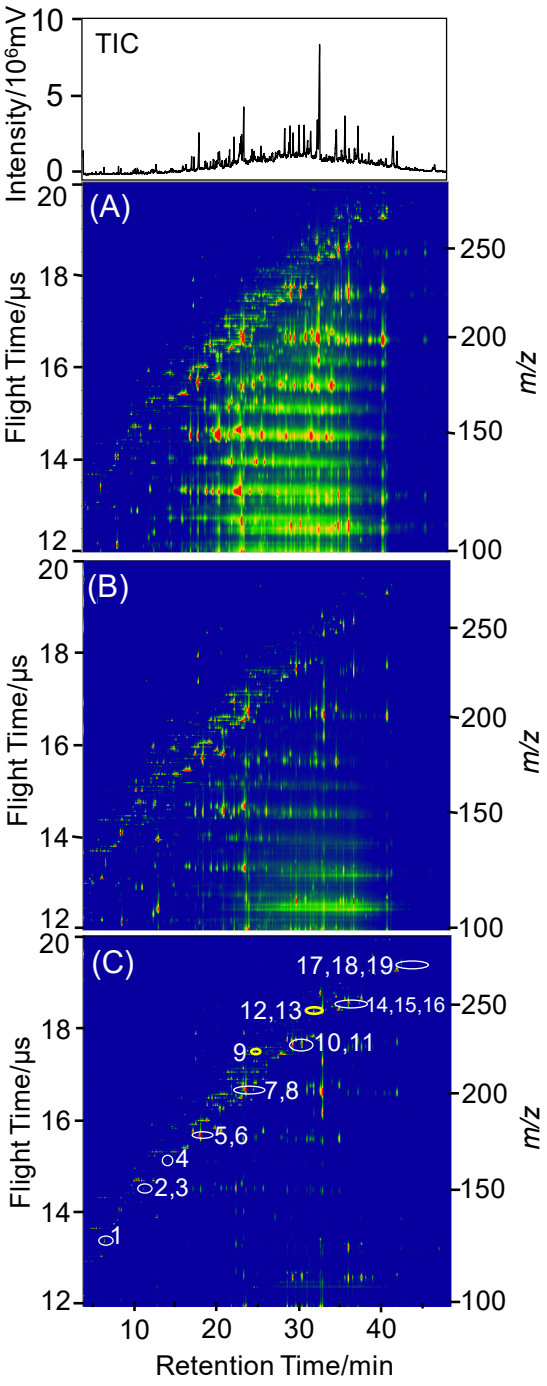

Fig. 7 A. Li et al.

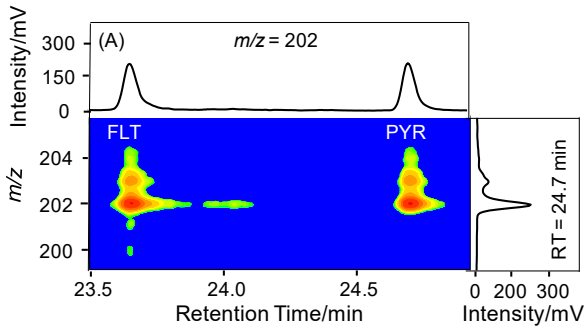
Intensity/mV
300
150
0
(A)
m/z = 202
FLT
PYR
m/z
204
202
200
23.5
24.0
24.5
Retention Time/min
RT = 24.7 min
0 200 300
Intensity/mV

For TOC